Total kinetic energy release in the fast-neutron-induced fission of ^{237}Np

A. Pica,[1] A. T. Chemey,[1] L. Yao,[1] W. Loveland,[1] H. Y. Lee,[2] and S. A. Kuvin[2]
[1]*Department of Chemistry, Oregon State University, Corvallis, Oregon 97331, USA*
[2]*Physics Division, Los Alamos National Laboratory, Los Alamos, New Mexico 87545, USA*

(Received 22 September 2020; accepted 10 November 2020; published 11 December 2020)

The total kinetic energy (TKE) release in the fast neutron-induced fission of ^{237}Np was measured for neutron energies from $E_n = 2.6$–100 MeV at the Los Alamos Neutron Science Center at the Weapons Neutron Research facility. The post-TKE release decreases nonlinearly with increasing incident neutron energy and can be represented as TKE (MeV) $= (174.38 \pm 0.72)$–$(5.11 \pm 0.5821)\log_{10}E_n$ for $E_n > 1$ MeV. Analysis of the fragment mass distributions indicates that the decrease in TKE with increasing E_n is a consequence of the fading out of shell effects at high excitation energies (resulting in an increase of symmetric fission) and the decrease of the total kinetic energy associated with asymmetric fission with increasing E_n.

DOI: 10.1103/PhysRevC.102.064612

I. INTRODUCTION

The fission process emits an enormous amount of energy per event, on the order of 200 MeV per nucleus for actinides. The majority of the energy released in the fission of actinide nuclei appears in the form of the kinetic energy of the two fission fragments. According to the conservation of momentum, the partitioning of energy between the two fragments is dependent on their masses; the lighter fragment garners more kinetic energy than its heavier counterpart. The sum of the two fragments' kinetic energy is the total kinetic energy (TKE). The TKE is an important fundamental feature of fission, and studies of TKE can help to elucidate some of the physics behind the large-scale collective motion of the nucleus.

Two factors dictate the magnitude of the TKE release. The first is the large Coulomb repulsion between the protofragments at the scission point, and the second is the conversion of the collective energy of the nucleus to kinetic energy of the fragments as the nucleus transitions from the saddle point to the scission point. We can use the first factor to perform a first approximation of the kinetic energies of the fission fragments. Based on Coulomb repulsion we can write TKE as a function of the fragments charge and radius, assuming $R = r_0 A^{1/3}$,

$$\mathrm{TKE} \approx \frac{Z_1 Z_2 e^2}{r_0\left(A_1^{1/3} + A_2^{1/3}\right)}. \tag{1}$$

Equation (1) is based upon the Coulomb forces acting on the fragments. Although this equation is reasonable at making first-order approximations of TKE, it slightly overestimates the impact of Coulomb repulsion because the equation assumes the protofragments are spheres at the scission point. In reality, they are highly deformed. Such deformation means the protofragments are more distant from each other at the scission point and, therefore, experience less Coulomb repulsion. A more widely used empirical equation is as follows:

$$\mathrm{TKE} \approx \frac{(0.1189 \pm 0.0011)Z^2}{A^{1/3}} + 7.3 \pm 1.5\,\mathrm{MeV} \tag{2}$$

obtained by Viola *et al.* [1] where the second term represents the conversion of energy stored in deformation to kinetic energy.

Previous studies of ^{237}Np (n, f)

Although the TKE for thermal neutron-induced fission has been extensively studied in many actinide systems, the same cannot be said for high incident neutron energies. There have been a limited number of studies on the ^{237}Np (n, f) reaction [2,3] in which TKE release and mass distributions were reported. These studies are summarized in Table I. Until this paper, there have been no measurements made of the ^{237}Np (n, f) reaction for $E_n > 5.5$ MeV. As such the measurements presented in this paper substantially extend our knowledge of the TKE release for the ^{237}Np (n, f) reaction.

II. EXPERIMENT

This experiment was carried out using the 15R beamline at Los Alamos National Laboratory, Los Alamos Neutron Science Center at the Weapons Neutron Research (LANSCE-WNR) facility over a 7-day period in December 2019. The LANSCE-WNR provides a high fluence of "white spectrum" neutrons generated by spallation of a thick tungsten target by 800-MeV protons, producing $\approx 10^5$–10^6 n/s up to $E_n = 100$ MeV [4,5]. The proton beam consists of 625-μs macropulses. Each macropulse is composed of 250-ps-wide micropulses that are spaced 1.8 μs apart. The macropulses had a repetition rate of 100 Hz. The pulsed nature of the proton beam enables the measurement of the time-of flight (energy) of the incident neutrons.

TABLE I. Previous work on the ^{237}Np (n, f) reaction.

E_n range (MeV)	Reference
0.3–5.5	[3]
0.8 and 5.5	[2]

The general arrangement of the experiment is shown in Fig. 1. The neutron flight path, i.e., the distance from the spallation source to the ^{237}Np target, was measured to be 13.85 m. The neutron beam was collimated to a 1-cm diameter. An evacuated thin-walled aluminum scattering chamber held the ^{237}Np target and the Si PIN diode fission detectors. At the end of the 7-day irradiation period, a total of 8618 coincident fission events were detected.

A. Target preparation

Targets containing actinide nuclei can be produced via molecular plating, electroplating, or vapor deposition. Vapor deposition was chosen as the target making method to ensure a uniform NpF_4 surface without the presence of "crud" from cracked solvent molecules which can affect the uniformity of molecular plated targets [6]. The 1-cm-radius target contained 34.2-μg/cm^2 ^{237}Np F_4 (measured by α spectroscopy) that was deposited on an $\approx$100-μg/cm^2 carbon foil. The target was tilted 45 ° with respect to the incident beam.

B. Fission detectors

The scattering chamber was aligned with the neutron beam using a combination of neutron-exposed photoplates and an alignment laser. Inside the scattering chamber, two arrays of nine Si PIN photodiodes (Hamamatsu S3590-09), arranged in a 3 × 3 array, were used to detect the fission products. The arrays were arranged on opposite sides of the beam at angles of 65 ° and 115 ° with respect to the incident beam. Each individual PIN diode had an area of 1 cm^2, and the detectors were placed 3.5 cm from the actinide target. Coincident fission fragments in both the left and right arrays were required to process a signal. The pulse height defect of the detectors for fission fragments was determined by applying the Schmitt method [7] to the known fission spectra of ^{252}Cf. The fragment energy loss in the actinide deposit and the carbon foil target backing was determined by the Northcliffe- Schilling energy loss tables on an event by event basis [8].

The time of flight of each interacting neutron was measured using a timing pulse from a Si PIN diode and the accelerator RF signal. The neutron energies were calculated based on the relativistic relationship between the distance traveled by the neutrons, the position of the photofission peak in the fission time-of-flight spectrum, and the observed time difference between the neutron timing signal and the accelerator RF signal [9]. The position of the photofission peak was measured to have an uncertainty of 0.24 ns with a relative uncertainty of 0.52%. The 1.8-μs proton pulse rate allowed for a small fraction of "wrap around" neutrons to reach the scattering chamber among the neutrons of the previous pulse. Accordingly, these neutrons would either be of very high energy, or very low energy. For the 13.85-m flight-path used in this experiment, the low-energy wrap around neutrons would have $E_n < 0.4$ MeV. The near-negligible cross section for the ^{237}Np (n, f) reaction at this energy means that these low-energy wrap around neutrons were ignored. Similarly, the high-energy wrap around neutrons would be of sufficient energy as to appear with the slowest neutrons from the previous beam burst. Wrap around events of this nature set the lower limit for the neutron energy resolution. Since no events below the fission threshold of $E_n \leqslant 0.7$ MeV [10] were detected, the high-energy wrap around neutrons were also ignored. The neutron energies were binned logarithmically to give bins of equal associated uncertainty for the neutron energy.

C. The 2*E* method

The 2E method was used to measure the fission product masses and their TKE by detecting the fission products and determining their energies after neutron emission. (We use the convention that the term "fission fragments" refers to preneutron emission whereas the term "fission product" refers to postneutron emission.) Conservation of momentum and mass for the coincident fission products gives

$$M'_H V'_H = M'_L V'_L, \tag{3}$$

$$M'_L + M'_H = M_{\mathrm{CN}}, \tag{4}$$

$$M'_H E'_H = M'_L E'_L. \tag{5}$$

$$M'_L = M_{\mathrm{CN}} \frac{E'_H}{E'_H + E'_L}, \tag{6}$$

where H represents the heavy fragment, L represents the light fragment, CN represents the compound nucleus, and " ′" indicates a quantity that pertains to preneutron emission. Our detection apparatus, due to the subfemtosecond timescale of the compound nucleus' descent to scission, measures

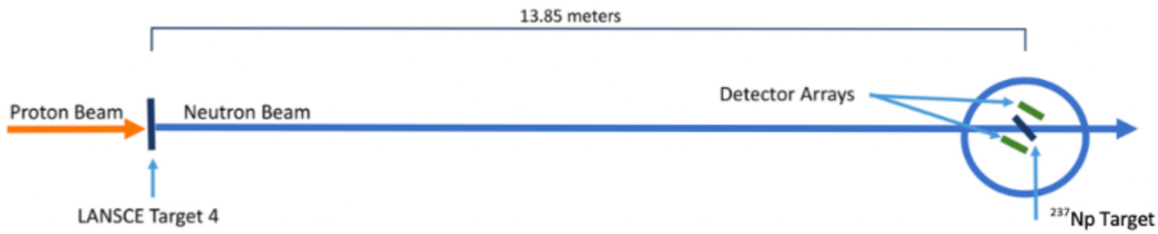

FIG. 1. Schematic of the detection setup at the LANSCE facility.

TABLE II. TKE and $\sigma^2_{\text{post TKE}}$ in the ^{237}Np (n, f) reaction as a function of incident neutron energy. The neutron bin limits are given in the first column whereas the second column is the geometric mean of the neutron energies. The last column is the number of events N in the bin.

E_n range (MeV)	E_n (MeV)	$_{\text{post}}$TKE (MeV)	$_{\text{pre}}$TKE (MeV)	σ^2_{post} (MeV^2)	Events
2.60–3.31	2.96	170.8 ± 0.4	173.1 ± 0.4	92.8 ± 0.3	887
3.32–4.38	3.83	171.6 ± 0.4	173.8 ± 0.4	91.4 ± 0.3	868
4.39–6.09	5.19	171.0 ± 0.4	173.6 ± 0.4	89.4 ± 0.3	865
6.10–8.06	7.06	171.2 ± 0.4	173.3 ± 0.4	109.8 ± 0.4	861
8.07–11.66	9.7	170.2 ± 0.4	172.2 ± 0.4	108.0 ± 0.3	867
11.67–18.56	14.8	168.0 ± 0.4	170.9 ± 0.4	109.6 ± 0.4	861
18.57–29.66	23.9	167.1 ± 0.4	169.5 ± 0.4	107.3 ± 0.4	863
29.67–45.72	37.1	164.9 ± 0.4	167.5 ± 0.4	118.9 ± 0.4	862
45.73–68.78	56.5	166.0 ± 0.4	168.6 ± 0.4	113.9 ± 0.4	870
68.79–100	83.8	164.8 ± 0.5	168.0 ± 0.4	126.3 ± 0.4	814

postneutron evaporation fission products [11]. Determination of mass yields required preneutron evaporation masses. To account for neutron evaporation, we used a common approximation for prompt neutron multiplicity as a function of excitation energy and postneutron fragment mass. We, therefore, made the following corrections for neutron emission,

$$E'_{L,H} = E_{L,H}\left(1 + \frac{\upsilon_{\text{post}}(m'_{L,H})}{m_{L,H}}\right), \tag{7}$$

$$m_{L,H} = m'_{L,H} - \upsilon_{\text{post }L,\,H}(E_n,\ m'_{L,H}), \tag{8}$$

where υ_{post} (A) is the postfission prompt neutron multiplicity calculated from the general description of fission observables (GEF) model at particular E_n [10,12]. In the laboratory system postneutron emission fission product energies $(E_{L,H})$ are calculated by correcting the measured fission product energies for detector pulse height defects and fission product energy losses in the target material and backing [9]. To deduce the postneutron emission mass distributions an iterative correction procedure [13] was applied. This iterative procedure assumed zero charged particle emission and ceased when the differences in fragment mass between iterations was less than 0.1 u.

D. Corrections for pulse height defect and fragment energy loss

We measured, on an event by event basis, the pulse heights of the coincident fission fragments. To accurately transform these pulse heights into energies, we had to account for the pulse height defect (PHD). A PHD occurs when a fission fragment strikes the PIN diode with such a high rate of energy loss that recombination occurs in the tracks of the incident particle along with any losses of energy in the detector dead layer. To make corrections for this effect we applied the Schmitt method [7]. The Schmitt method exploits the known fission spectra of ^{252}Cf to determine a set of constants that describe the PHD for a given detector. For Si surface barrier detectors, the magnitude of the PHD generally ranges from 3 to 13 MeV [14–16]. The energy loss of the fission products in the target deposit and the carbon foil were calculated using the Northcliffe-Schilling tables [8]. Typically, 5–10% of the total fission product energy is lost in the target backing [17].

III. RESULTS

In Table II, we report the pre- and postneutron TKEs and their variances as a function of incident neutron energy for the ^{237}Np (n, f) reaction. This data set significantly increases the range of energies studied compared to previous measurements that only explored this reaction to a maximum value of 5.5 MeV in neutron energy [2,3]. In Fig. 2, we present the postneutron evaporation TKE distributions sorted by the neutron energy bin. The data were binned as to have a similar number of events per neutron energy bin. The thin red lines in each plot represent the results of fitting the data with Gaussian distributions.

A. TKE vs E_n

In Fig. 3, we show the $_{\text{post}}$TKE response up to $E_n = 6$ MeV from this paper and that documented in the literature [2,3]. In doing so, we restrict our attention to systems where only first chance fission is expected. We found the TKE released in the low E_n energy range to be ≈1.7 and 0.9 MeV higher than that reported by Hambsch *et al.* [3] and Naqvi *et al.* [2], respectively. It is important to note that Hambsch *et al.* [3] normalized their data to a ^{235}U preneutron TKE of 179.5 MeV, a value of ≈0.5 MeV lower than the most current compilation of Madland [18]. Similarly, Naqvi *et al.* [2] compared their ^{237}Np TKE data to a ^{235}U postneutron TKE value of 167.45 MeV. This value is 1.7 MeV lower than what is reported by Madland [18]. As a result, both the data of Naqvi *et al.* [2] and Hambsch *et al.* [3] likely underestimate the TKE release in ^{237}Np.

The $_{\text{post}}$TKE release for the fast neutron-induced fission of ^{237}Np over the entire measured energy range is shown in Fig. 4 for the present data as well as comparisons to other ^{237}Np (n, f) reaction data and the GEF model. The overall trend of decreasing TKE with increasing excitation is consistent with other fast neutron TKE studies of actinides [17,19–27]. Although the TKE release for the lowest-energy neutrons is approximately linear, a first-order $\log_{10}(E_n)$ polynomial fit is needed to describe the fast neutron energy region ($E_n >$ 1 MeV). The fit to our data (Fig. 4) is given by the equation TKE = (174.38 ± 0.72)–(5.11 ± 0.5821)$\log_{10}E_n$.

An interesting feature apparent in Fig. 4 is a "bump" in TKE in the $E_n = 46$–69 MeV energy bin. This

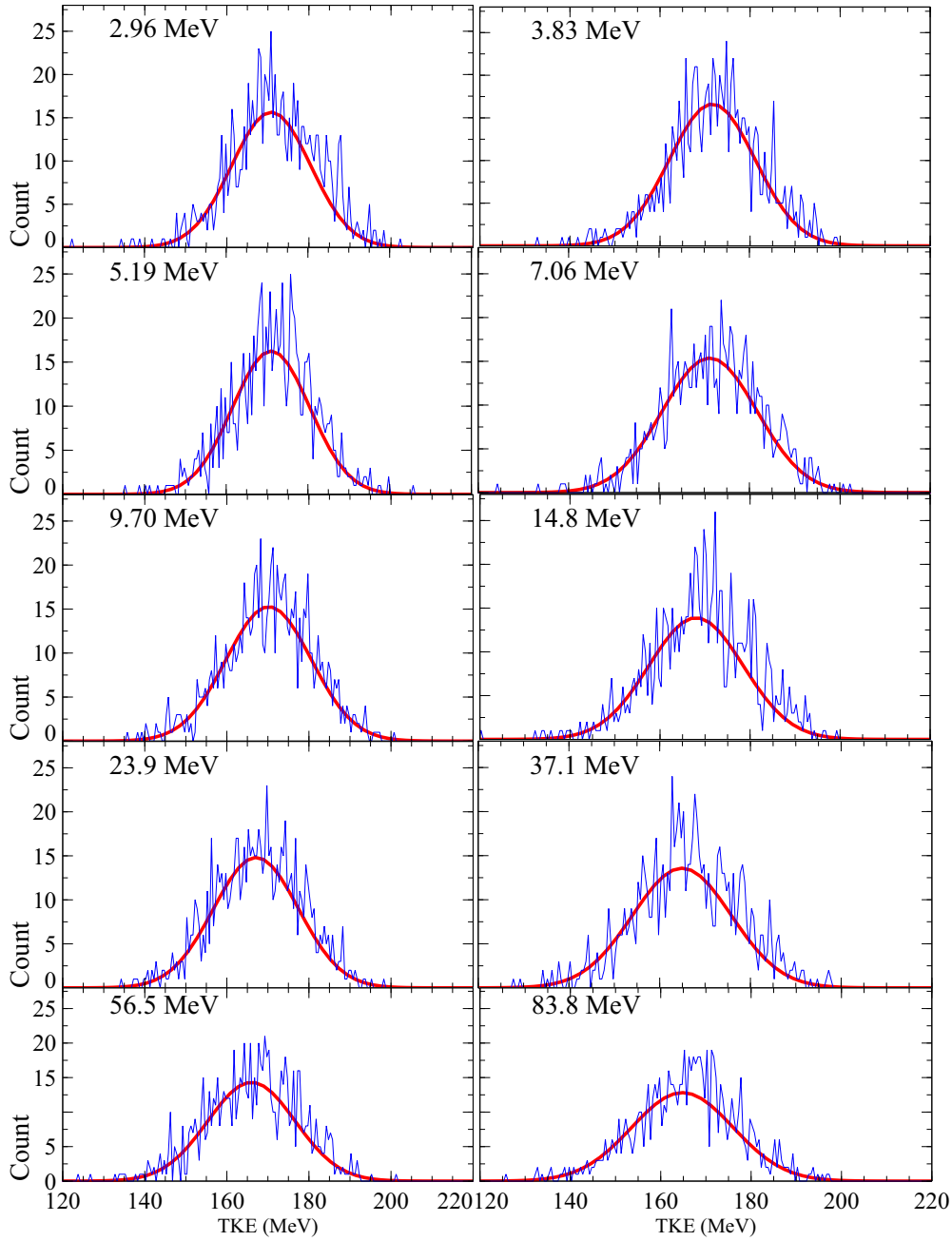

FIG. 2. The post-TKE distributions sorted into the energy bins described in Table II are plotted. The plotted curves (red lines) represent the results of fitting the distributions with Gaussian functions.

peculiar bump has been observed in other actinides within this neutron energy range, particularly, with ^{232}Th, ^{235}U, and ^{239}Pu [17,19,26]. This anomaly is not predicted in models. The observation of such a bump across several actinides suggests either a systematic flaw in our measurement or a gap in our understanding of nuclear physics in this energy range.

B. $_{\text{post}}$TKE comparison to the GEF model

When comparing the GEF model $_{\text{post}}$TKE values to those measured in this paper, GEF systematically overestimates $_{\text{post}}$TKE by $\approx$1.2% for all data points in the region $E_n \leqslant 50$ MeV. This is equivalent to approximately 2 MeV per energy bin (Fig. 4). This overestimation is likely the result of the GEF model misattributing a small fraction of the energy of the fissioning ^{237}Np nucleus to the kinetic energy of the fission products instead of particle evaporation. A study of the high-energy fission of ^{235}U(n, f) found that the GEF framework routinely underestimated the total neutron evaporation by 5–10% for $E_n = 0$–50 MeV [19]. A similar underestimation is seen for the ^{239}Pu (n, f) reaction where the GEF prompt neutron multiplicity underestimates the known values for $A > 147$, and/or $E_n > 12$ MeV [28–32].

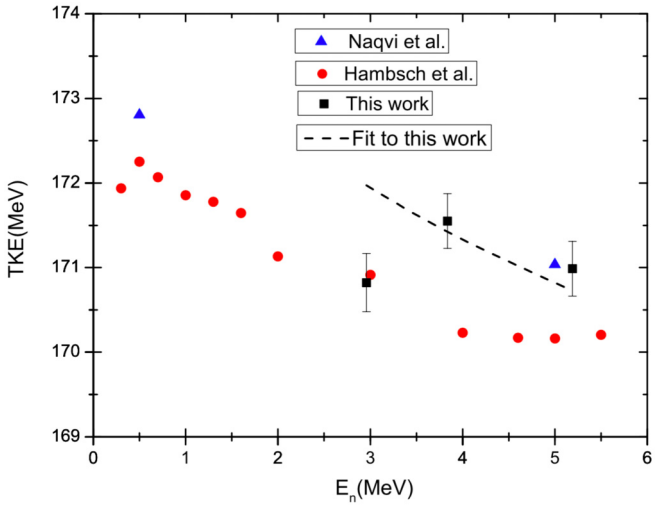

FIG. 3. Comparison of the average post-TKE measured for the ^{237}Np (n, f) reaction as a function of incident neutron energy measured in this paper to previous studies and a fit to our data (dashed line) from 2.6 to 100 MeV.

The GEF model underestimates the $_{\text{post}}$TKE for $E_n >$ 50 MeV by ≈0.7% or 1.1 MeV. This transition from the GEF model overestimation to sudden underestimation is due to the bump in the experimental data and further highlights the importance of being able to understand this anomaly.

C. TKE distribution variances (σ)

The results of fitting the TKE data with Gaussian distributions are shown in Fig. 2, and the resulting variances are sensitive markers of multichance fission. At energies where multichance fission is possible, a new fission pathway opens, and the presence of this new channel is reflected in the broadening of the Gaussian distribution. This phenomenon is well documented, particularly, in ^{235}U (n, f) studies [19,33]. In Fig. 5, we limit our attention to measured variances

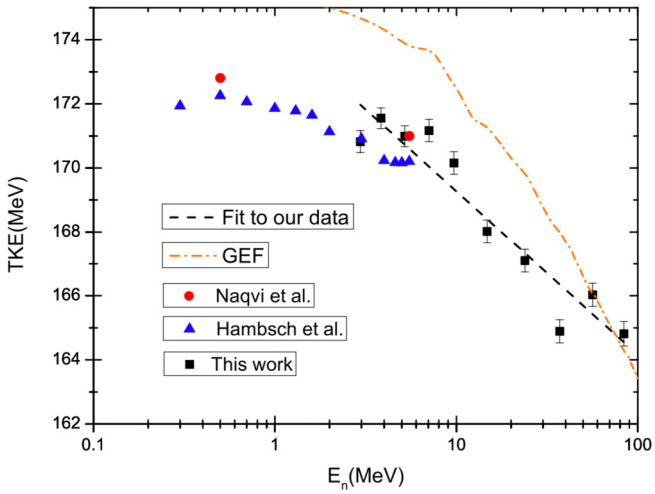

FIG. 4. Postneutron TKE released for the ^{237}Np (n, f) reaction from E_n = 0.3–100 MeV. TKE error bars are statistical.

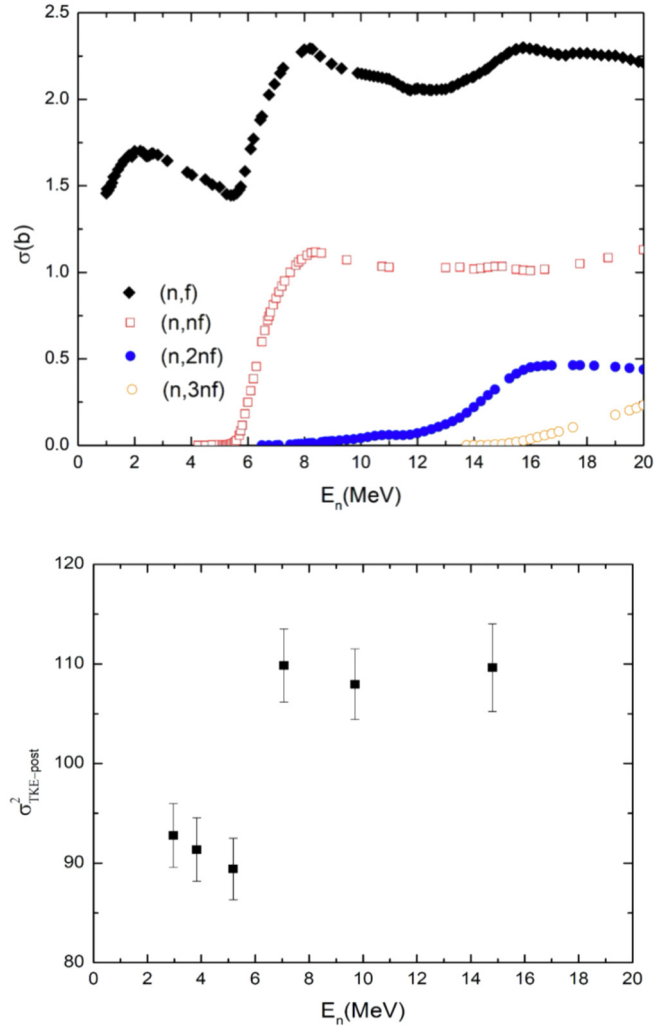

FIG. 5. Top: cross section for ^{237}Np (n, f) from evaluated nuclear data file (ENDF)/B-VIII and ENDF/B-VI. Bottom: measured TKE σ^2 vs E_n for this paper.

below 20 MeV to highlight the dependence of the measured variances of the TKE distributions on the number of fission channels present. As expected, we see a significant increase in the measured variance at the onset of second chance fission ≈7 MeV.

D. Mass yield distributions

In actinide fission, the fission fragment mass distribution is bimodal at low excitation energies. As E_n is increased the valley between the asymmetric fission peaks begins to fill. In Fig. 6 we plot the mass distributions measured in this paper, normalized to 200%, and the predictions of the GEF model. The resolution of our measurement is ± 5 u. It is evident in Fig. 6 that as E_n increases the two asymmetric peaks merge reflecting the emergence of symmetric fission. The rate of symmetric ingrowth and its relative proportion to the total number of events are in excellent agreement with that predicted by GEF [10].

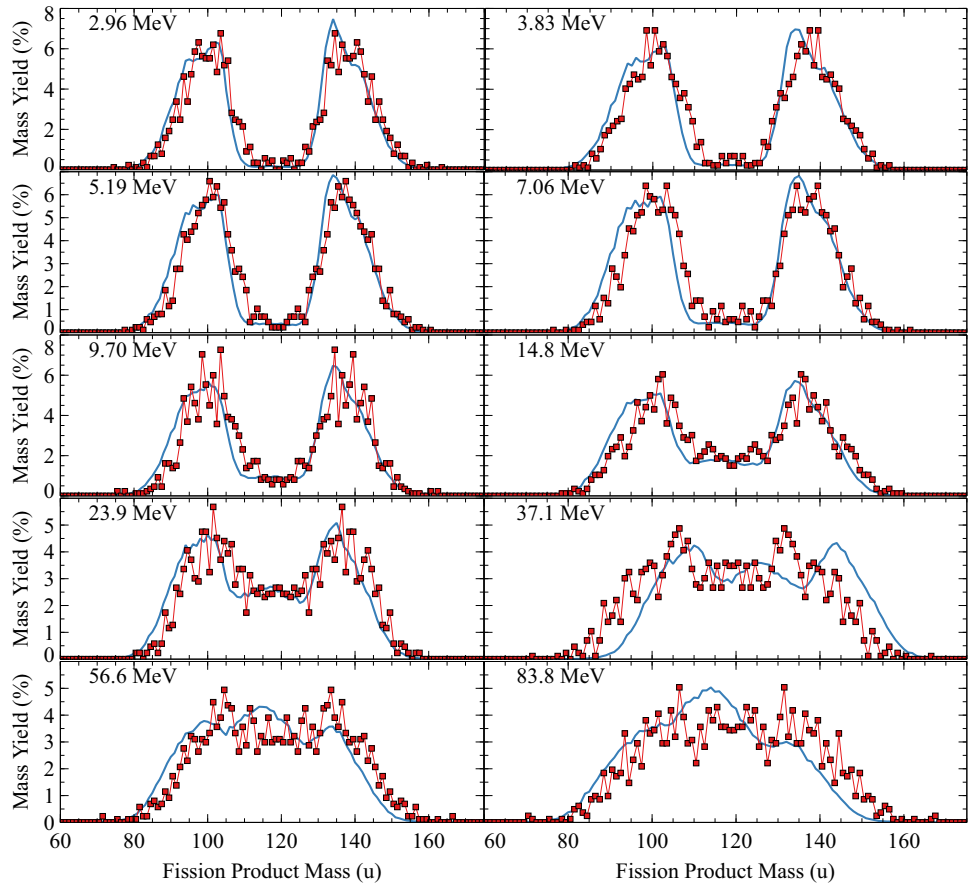

FIG. 6. Comparison of the mass distributions measured in this paper (red squares), normalized to 200%, and the predictions of the GEF_{post} model (blue line) [10].

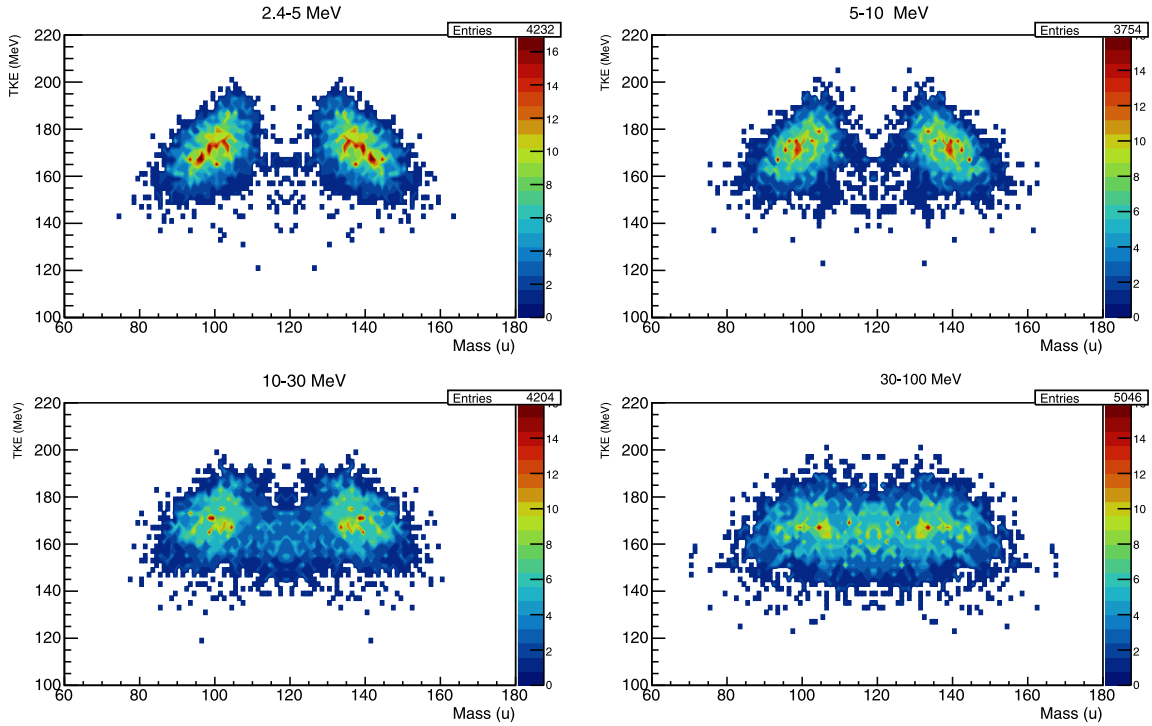

FIG. 7. ^{237}Np (n, f) product mass TKE distributions at various E_n's.

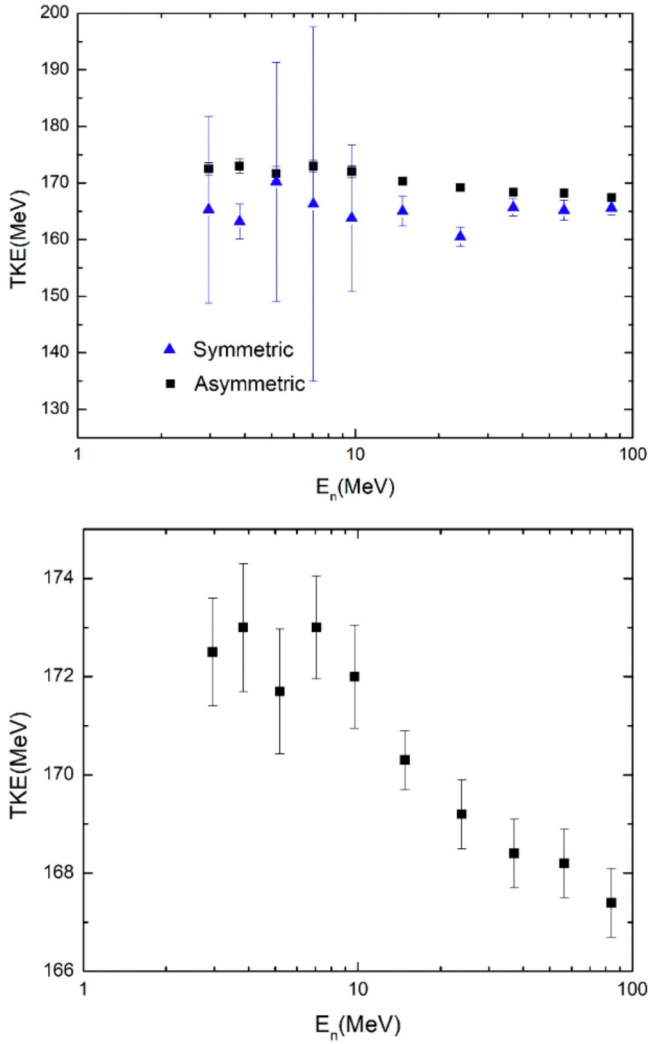

FIG. 8. (Top) TKE vs E_n with fission events separated into symmetric and asymmetric events. (Bottom) Dependence of asymmetric TKE events on neutron energy.

It is well documented in the literature [34] that the constancy of the heavy fragment mass peak is due to the influence of the spherical $N = 82$ and deformed $N = 88$ neutron shells and $Z = 50$ proton shell. In this system the mass of the heavy fragment is anchored at ≈139.4 u. This is in agreement with Ref. [3].

Fission channel symmetry and TKE

It has been demonstrated in many actinide systems that the general trend of decreasing TKE with increasing excitation is a consequence of the increasing probability of symmetric fission as E_n increases. For low-energy neutron-induced fission, asymmetric fission dominates due to nuclear shell effects. As E_n increases, symmetric fission begins to emerge, and eventually, symmetric fission dominates. Figure 7 shows the fragment mass and TKE distributions for ^{237}Np at various energies. At the lowest neutron energies, the fission mass distribution is almost purely asymmetric. As E_n increases, more fission fragments with $A = 120$ are detected indicating a symmetric fission event.

The symmetry of the fissioning system was determined via the calculated masses of the fission products. For an event to fall into the asymmetric bin, the following condition had to be met for one of the fission fragments:

$$A_{\text{range}} = \left(\frac{A_{\text{CN}} - \upsilon_{\text{tot},\,E_n}}{2} + 20\right) \pm 5\,\text{u}, \tag{9}$$

where $\upsilon_{\text{tot},E_n}$ is the total neutron multiplicity as calculated by GEF [10] at the corresponding E_n. The second term (+20) is the calculated difference between the A_H peak in asymmetric fission and the single peak corresponding to symmetric fission. If both fission products fall within a finite mass range (S_{range}) the event passed into the symmetric bin, where S_{range} is defined as

$$S_{\text{range}} = \frac{A_{\text{CN}} - \upsilon_{\text{tot},E_n}}{2} \pm 5\,\text{u}. \tag{10}$$

In Fig. 8 (top), we show the TKE_{sym} and TKE_{asym} events and plot them against E_n. In Fig. 8 (bottom) we see that TKE_{asym} drops off rather sharply above $E_n = 10$ MeV. Across the entire measured E_n range, TKE_{asym} decreased from 172.5 to 165.6 MeV. However, the TKE release remained virtually constant. This suggests that the overall trend of decreasing TKE is not exclusively a consequence of the onset of symmetric fission but is instead also impacted by a decreasing TKE_{asym} as well. Hambsch *et al.* [3] theorized that this decreasing asymmetric TKE trend observed in the ^{237}Np(n, f) reaction could involve a more drastic deformation of fission fragments, particularly for $130 < A < 145$ range as E_n increases [3]

IV. CONCLUSION

Previous TKE studies of ^{237}Np (n, f) are limited and were restricted to incident neutron energies less than 6 MeV. The goal of this paper was to build upon the existing TKE data available for ^{237}Np by extending measurements into the fast neutron energy range up to 100 MeV.

A vapor deposited $^{237}\text{Np}\,\text{F}_4$ target was irradiated at LANSCE-WNR to measure the TKE dependence for the ^{237}Np (n, f) reaction from $E_n = 2.6$–100 MeV. The TKE values reported in this paper were compared to that of Refs. [2,3] and the prediction of the GEF model [10]. We also report fission fragment mass distributions and gained additional detail about the fissioning system by separating the fission path by symmetry regimes. We attribute the observed trend of decreasing TKE to the emergence of symmetric fission as well as the rapid drop off of TKE_{asym} as excitation increases. The peculiar bump in TKE at $E_n = 45$–70 MeV, whereas consistent with other actinide studies within this framework, is not yet understood and needs further exploration.

[1] V. E. Viola, K. Kwiatkowski, and M. Walker, Phys. Rev. C **31**, 1550 (1985).

[2] A. A. Naqvi, F. Käppeler, F. Dickmann, and R. Müller, Phys. Rev. C **34**, 218 (1986).

[3] F. J. Hambsch, F. Vivès, P. Siegler, and S. Oberstedt, Nucl. Phys. A **679**, 3 (2000).
[4] P. W. Lisowski, C. D. Bowman, G. J. Russell, and S. A. Wender, Nucl. Sci. Eng. **106**, 208 (1990).
[5] P. W. Lisowski and K. F. Schoenberg, Nucl. Instrum. Methods Phys. Res., Sect. A **562**, 910 (2006).
[6] M. J. Silveira, A. Pica, and W. Loveland, Nucl. Instrum. Methods Phys. Res., Sect. A **982**, 164570 (2020).
[7] H. W. Schmitt, J. H. Neiler, and F. J. Walter, Phys. Rev. **141**, 1146 (1966).
[8] L. C. Northcliffe and R. F. Schilling, Atomic Data and Nuclear Data Tables **7**, 233 (1970).
[9] J. W. King, Ph.D. thesis, Oregon State University, 2018.
[10] K. H. Schmidt and B. Jurado, khs.erzhausen.de (version of the model that used GEF2019/1.3 downloaded May 2019).
[11] W. Loveland, D. J. Morrissey, and G. T. Seaborg, *Modern Nuclear Chemistry* (Wiley, Hoboken, NJ, 2017).
[12] K. H. Schmidt, B. Jurado, C. Amouroux, and C. Schmitt, Nuclear Data Sheets **131**, 107 (2016).
[13] V. Simutkin, Ph.D. thesis, Uppsala University, 2010.
[14] M. Ogihara, Y. Nagashima, W. Galster, and T. Mikumo, Nucl. Instrum. Methods Phys. Res., Sect. A **251**, 313 (1986).
[15] T. Kitahara, H. Geissel, Y. Laichter, and P. Armbruster, Nucl. Instrum. Methods **196**, 153 (1982).
[16] S. B. Kaufman, E. P. Steinberg, B. D. Wilkins, J. Unik, A. J. Gorski, and M. J. Fluss, Nucl. Instrum. Methods **115**, 47 (1974).
[17] J. King, R. Yanez, W. Loveland, J. S. Barrett, B. Oscar, N. Fotiades, F. Tovesson, and H. Y. Lee, Eur. Phys. J. A **53**, 238 (2017).
[18] D. G. Madland, Nucl. Phys. **A772**, 113 (2006).
[19] R. Yanez, J. King, J. S. Barrett, W. Loveland, N. Fotiades, and H. Y. Lee, Nucl. Phys. A **970**, 65 (2018).
[20] D. Higgins, U. Greife, F. Tovesson, B. Manning, D. Mayorov, S. Mosby, and K. Schmitt, Phys. Rev. C **101**, 014601 (2020).
[21] A. Al-Adili, F. J. Hambsch, S. Pomp, S. Oberstedt, and M. Vidali, Phys. Rev. C **93**, 034603 (2016).
[22] A. Al-Adili, F. J. Hambsch, S. Pomp, and S. Oberstedt, Phys. Rev. C **86**, 054601 (2012).
[23] F. J. Hambsch, S. Oberstedt, A. Al-Adili, T. Brys, R. Billnert, C. Matei, A. Oberstedt, P. Salvador-Castiñeira, A. Tudora, and M. Vidali, Nuclear Data Sheets **119**, 38 (2014).
[24] R. Müller, A. A. Naqvi, F. Käppeler, and F. Dickmann, Phys. Rev. C **29**, 885 (1984).
[25] C. Straede, C. Budtz-Jørgensen, and H. H. Knitter, Nucl. Phys. **A462**, 85 (1987).
[26] K. Meierbachtol, F. Tovesson, D. L. Duke, V. Geppert-Kleinrath, B. Manning, R. Meharchand, S. Mosby, and D. Shields, Phys. Rev. C **94**, 034611 (2016).
[27] D. L. Duke, F. Tovesson, A. B. Laptev, S. Mosby, F.-J. Hambsch, T. Bryś, and M. Vidali, Phys. Rev. C **94**, 054604 (2016).
[28] A. Tudora, F.-J. Hambsch, and V. Tobosaru, Nucl. Sci. Eng. **192**, 52 (2018).
[29] C. Tsuchiya, Y. Nakagome, H. Yamana, H. Moriyama, K. Nishio, I. Kanno, K. Shin, and I. Kimura, J. Nucl. Sci. Technol. **37**, 941 (2000).
[30] K. Nishio, Y. Nakagome, I. Kanno, and I. Kimura, J. Nucl. Sci. Technol. **32**, 404 (1995).
[31] V. F. Apalin, Y. N. Gritsyuk, I. E. Kutikov, V. I. Lebedev, and L. A. Mikaelian, Nucl. Phys. **71**, 553 (1965).
[32] J. S. Fraser and J. C. D. Milton, Annu. Rev. Nucl. Sci. **16**, 379 (1966).
[33] D. L. Duke, Ph.D. thesis, Colorado School of the Mines, 2015.
[34] C. Wagemans, *The Nuclear Fission Process*, (CRC, Boca Raton, FL, 1991).